Chinese Chemical Letters 34 (2023) 108233

Contents lists available at ScienceDirect

Chinese Chemical Letters

journal homepage: www.elsevier.com/locate/cclet

Templated synthesis of imine-based covalent organic framework hollow nanospheres for stable potassium-ion batteries

Jianlu Sun, Ruiqi Tian, Yuehua Man, Yating Fei, Xiaosi Zhou*

School of Chemistry and Materials Science, Nanjing Normal University, Nanjing 210023, China

ARTICLE INFO

Article history:
Received 28 December 2022
Revised 16 January 2023
Accepted 15 February 2023
Available online 19 February 2023

Keywords:
Potassium ion batteries
Anode
Covalent organic framework
Templated synthesis
Hollow nanospheres

ABSTRACT

Covalent organic frameworks (COFs), as highly tunable porous crystalline materials, have promising applications in potassium-ion batteries (PIBs) due to their abundant charge carrier transport channels and excellent structural stability. However, the excessive stacking of interlayer electron clouds makes it difficult to expose internal active sites. Strategies to design functional COFs with controllable morphology and copious active sites are promising but still challenging. Herein, by utilizing the condensation between 1,3,5-triformylbenzene (TFB) and *p*-phenylenediamine (PPD) and using amino-modified SiO_2 nanospheres as templates, we synthesize core-shell NH_2-SiO_2@TP-COF. Through NaOH etching of NH_2-SiO_2@TP-COF, we obtain imine-based TP-COF hollow nanospheres, which shows excellent potassium storage performance when applied to the anode for PIBs. *Ex-situ* analysis and density functional theory calculations reveal that C=N groups and benzenes are active sites for K^+ storage.

With the continuous attention to fossil energy and environmental issues, energy-related technologies, especially secondary batteries, have been rapidly developed [1,2]. Lithium-ion batteries (LIBs) have attracted much attention due to their high energy density and long cycle life, but are currently limited by expensive lithium resources [3–5]. Potassium-ion batteries (PIBs) have a similar working mechanism to LIBs, with abundant potassium resources and higher conductivity of potassium electrolyte, which is conducive to rapid charge transfer [6–8]. As such, it has become a competitor of LIBs for large-scale applications [9,10].

However, due to the large ionic radius and high chemical reactivity of potassium ions and the poor interfacial stability associated with the electrolyte, considerable efforts have been devoted to developing suitable electrode materials [11–13]. Since the first report in 2005, covalent organic frameworks (COFs) have become a research hotspot owing to their firmness, orderliness, high designability, and smooth channels [14–16]. As a benefit of the stable chemical environment and rich electrochemical active sites, the high-speed charge transport channels of COFs have attracted the enormous attention of energy storage research [17].

To date, COFs have been extensively engineered, such as for morphological control, due to the low utilization of internal active sites caused by overlapping electron clouds between stacked layers for energy storage [18]. Hollow nanostructures have advantages in accelerating charge transport and exposing active sites [19–22]. Nevertheless, preparing functional hollow nanostructured COFs with controllable and uniform morphologies remains a great challenge [23–25]. Here, we use an amino-modified SiO_2 template (NH_2-SiO_2) to guide the condensation reaction between 1,3,5-triformylbenzene (TFB) and *p*-phenylenediamine (PPD) to obtain uniform TP-COF hollow nanospheres. The specially designed hollow architecture has a large exposed surface area and more active reaction sites. In addition, the COF hollow nanospheres can alleviate the electrode volume expansion during repeated cycling and achieve rapid electron/ion transportation reaction kinetics [26]. Notably, the obtained TP-COF hollow nanospheres manifest enhanced capacity (336 *vs.* 115 mAh/g at 0.1 A/g after 100 cycles), superior rate capacity (160 *vs.* 62 mAh/g at 1 A/g) and prolonged cycling stability (81.2% capacity retention after 500 cycles) compared with pristine TP-COF.

As shown in Fig. 1a, SiO_2 nanospheres were synthesized according to the Stöber method [27]. Subsequently, the surface of the SiO_2 nanospheres was functionalized by amino groups (NH_2-SiO_2) under the condition of (3-aminopropyl) triethoxysilane (APTES). Using NH_2-SiO_2 nanospheres as the template, the core-shell structure NH_2-SiO_2@TP-COF was formed through the condensation reaction of TFB and PPD. TP-COF hollow nanospheres (TP-COF HSs) were achieved by etching SiO_2 in NaOH solution. The chemical structure of TP-COF HSs is determined by Fourier transform infrared spectrometer (FTIR), X-ray diffraction (XRD), Raman spectroscopy, and X-ray photoelectron spectroscopy (XPS). The FTIR

* Corresponding author.
E-mail address: zhouxiaosi@njnu.edu.cn (X. Zhou).

https://doi.org/10.1016/j.cclet.2023.108233
1001-8417/

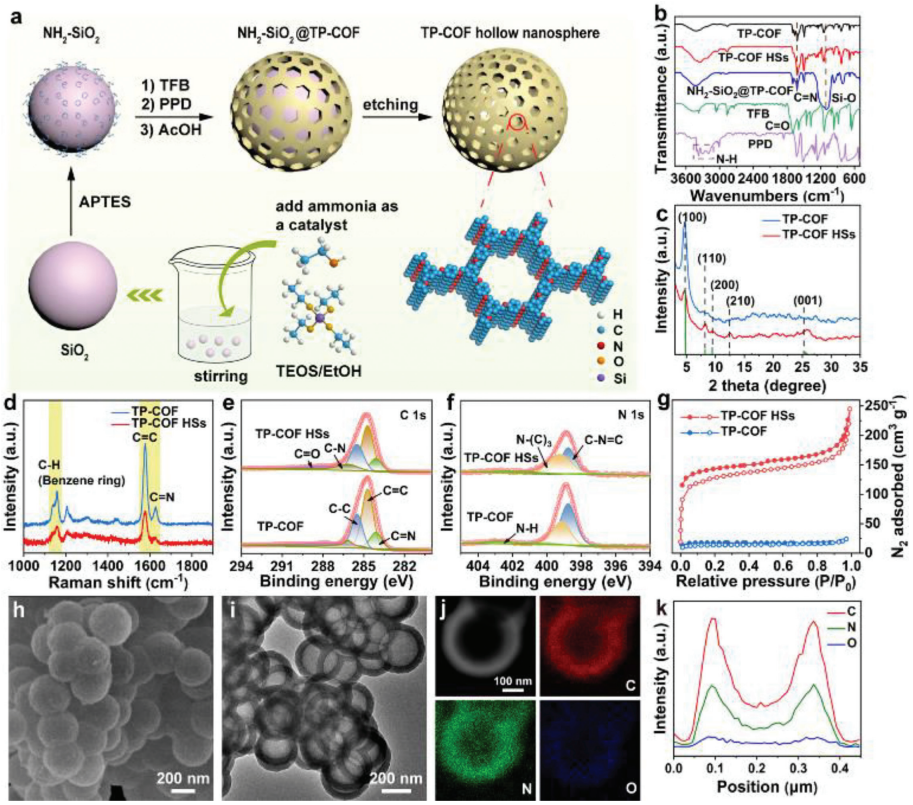

Fig. 1. (a) Schematic illustration of TP-COF HSs. (b) FTIR spectra of TP-COF, TP-COF HSs, NH_2-SiO_2@TP-COF, TFB and PPD. (c) XRD patterns, (d) Raman spectra, (e, f) C 1s and N 1s XPS spectra, and (g) N_2 adsorption-desorption isotherm of TP-COF HSs and TP-COF. (h) SEM image, (i) TEM image, (j) element mapping distributions, and (k) linear analysis of elements across TP-COF HSs.

spectra of TP-COF, NH_2-SiO_2@TP-COF, and TP-COF HSs display the stretching vibrations of the C=N bond at 1618 cm^{-1}, which confirms the successful synthesis of imine-based TP-COF (Fig. 1b) [28]. The peaks at ~1698 cm^{-1} and ~3380 cm^{-1} can be attributed to C=O and -NH_2 groups as terminal groups in TP-COF. The successful etching of SiO_2 in TP-COF HSs is supported by the disappearance of the 1105 cm^{-1} vibration belonging to Si–O in NH_2-SiO_2@TP-COF. Moreover, the diffraction peaks of TP-COF HSs are consistent with the fitting data, indicating that the template sacrificial strategy did not destroy the original crystal structure of TP-COF (Fig. 1c). The strong peak at 4.8° can be ascribed to the reflection of the (100) plane, while the weaker diffraction peaks of the (110), (200), (210) and (001) planes are located at 8.2°, 9.5°, 12.5° and 25.5°, respectively [29].

The composition of TP-COF HSs is further verified by Raman and XPS analysis. Bands corresponding to C=C and C=N groups around 1577 and 1628 cm^{-1} can be detected from TP-COF HSs (Fig. 1d) [30]. As illustrated in Fig. S1 (Supporting information), C, N and O elements can be clearly observed at 285, 398.4 and 531.8 eV in TP-COF HSs. The C 1s spectrum of TP-COF HSs (Fig. 1e) can be deconvoluted into five peaks at 288.1, 286.2, 285.5, 284.7 and 284.1 eV, corresponding to the C=O, C–N, C–C, C=C and C=N groups, respectively [31]. The peaks in the high-resolution N 1s spectrum (Fig. 1f) centered at 402.8, 399.1 and 398.8 eV are correlated to the N–H, N–C and N=C groups of TP-COF HSs, respectively [32]. This is in good agreement with the detection by FTIR (Fig. 1b). The specific surface area and pore diameter distribution of the samples were investigated by N_2 adsorption analysis (Fig. 1g and Fig. S2 in Supporting information). The surface area of TP-COF HSs is 485.7 m^2/g, which is much higher than that of TP-COF (41.3 m^2/g). The pores of both samples are concentrated at 1.7 nm, which is close to the theoretical value (Fig. S2) [30]. The larger specific surface area is beneficial to the penetration of electrolyte, endowing TP-COF HSs with better potassium storage performance. Thermal stability studies show that TP-COF HSs have good stability close to that of TP-COF, and they do not decompose significantly before 400 °C in N_2 (Fig. S3 in Supporting information).

The morphology of TP-COF HSs is compared with TP-COF, NH_2-SiO_2 template, and NH_2-SiO_2@TP-COF to demonstrate the formation of the hollow nanosphere structure by scanning electron microscopy (SEM) and transmission electron microscopy (TEM). As displayed in Fig. S4 (Supporting information), NH_2-SiO_2 shows a uniform solid spherical architecture with a smooth surface and a diameter of about 260 nm, similar to amorphous SiO_2. Fig. S5 (Supporting information) presents the rough profile of NH_2-SiO_2@TP-COF with a diameter of around 380 nm and a COF shell with a thickness of ~60 nm formed on NH_2-SiO_2. SEM and TEM images (Figs. 1h-k and Fig. S6 in Supporting information) clearly confirm the hollow structure of TP-COF HSs with rougher surface, while TP-COF demonstrates irregular solid nanospheres with an average diameter of approximately 600 nm (Fig. S7 in Supporting information). EDX line scan analysis of TP-COF HSs shows that C, N, and O elements are uniformly distributed in the COF shell (Fig. 1j), which suggests that SiO_2 is successfully etched with an obvious hollow structure. In contrast, SiO_2 without surface modification failed to form a core-shell structure under the same conditions (Fig. S8 in Supporting information). Therefore, the amino functionalization of the SiO_2 surface plays a pivotal role in the formation of the unique hollow architecture.

Cyclic voltammetry (CV) tests between 0.01 V and 3 V at 0.1 mV/s were employed to explore the redox reactions of TP-COF and TP-COF HSs as PIB anodes (Figs. 2a and b). The peak around

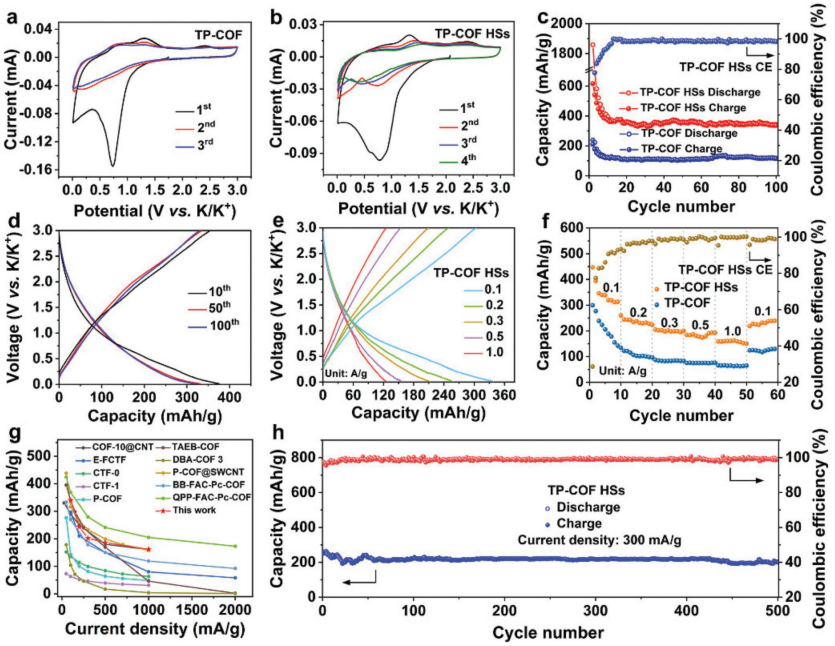

Fig. 2. CV curves for the first three cycles of (a) TP-COF and (b) TP-COF HSs. (c) Cycling performance of TP-COF and TP-COF HSs. (d, e) Selected discharge/charge profiles of TP-COF HSs. (f) Rate properties of TP-COF and TP-COF HSs. (g) Comparison of rate performance between TP-COF HSs and other COF electrodes. (h) Prolonged cycling stability of TP-COF HSs.

0.61 V in the first cycle corresponds to the production of a solid electrolyte interphase (SEI) film that disappears in the subsequent cycles [33,34]. A cathode peak at 0.75 V and an anode peak at 1.3 V can be identified, which correspond to K^+ uptake/removal processes, respectively. The potassium storage properties of TP-COF HSs and TP-COF at different current densities were characterized. After the capacity drops in the first few cycles, TP-COF HSs achieves a higher reversible capacity of 336 mAh/g after 100 cycles at 100 mA/g compared with TP-COF (115 mAh/g), thanks to the larger specific surface area and more exposed active site (Fig. 2c). The initial irreversible capacity loss of TP-COF HSs electrode also confirms the decomposition of electrolyte and the formation of SEI, which accords with the CV results. Furthermore, the reversibility of the TP-COF HS electrode is improved without significant capacity fading, and the Coulomb efficiency (CE) is gradually increased to about 100% (Fig. 2d). TP-COF and TP-COF HS electrodes exhibit off-plateau slopes in the discharge and charge curves associated with their 2D conjugate skeleton properties (Fig. S9 in Supporting information) [35]. It is worth mentioning that the hollow structure of TP-COF HSs basically maintained after 100 cycles, indicating effective strain release during battery cycling (Fig. S10 in Supporting information).

Figs. 2e and f show rate performance of the TP-COF HSs and TP-COF electrodes. When the current density increases from 0.1 A/g to 0.2, 0.3, 0.5 and 1.0 A/g, the reversible capacities of the TP-COF HS electrode are 330, 237, 201, 180 and 160 mAh/g, respectively, which are greater than those of TP-COF (205, 102, 82, 74 and 62 mAh/g). When the current rate returns to 0.1 A/g, the reversible potassium storage capacity of TP-COF HSs can be well recovered to 237 mAh/g (72%), while the K storage capacity of TP-COF is only 123 mAh/g (60%). In comparison with the published works, the electrochemical performance of TP-COF HSs has surpassed most of them (Fig. 2g and Table S1 in Supporting information). Due to the excellent thermal and chemical stability of TP-COF HSs, it is an ideal electrode material to achieve excellent long-term cycling stability. After activation, the TP-COF HS electrode renders a stable capacity of 203 mAh/g (81.2% capacity retention) after 500 cycles at 300 mA/g and an average CE near 100% (Fig. 2h).

To study the electrochemical behavior of TP-COF HS electrodes, CV with a scan rate of 0.1–1.0 mV/s, galvanostatic intermittent titration technique (GITT), and electrochemical impedance spectroscopy (EIS) were applied. CV curves at different scan rates were recorded to further investigate the K^+ storage behavior (Fig. 3a). A linear relation with a slope b value of 0.75/0.73 exists between the peak current and scan rate of TP-COF HSs, implying a coexistence of diffusion-dominated and capacitive-controlled potassium-ion storage processes (Fig. 3b). The capacitive contribution of the TP-COF HS electrode is 35.4% at 0.1 mV/s, which increases to 84.3% when the scan speed reaches 1.0 mV/s (Figs. 3c and d). TP-COF HSs exhibit a more pronounced capacitive-controlled process than TP-COF (Fig. S11 in Supporting information). The K^+ diffusion coefficient in TP-COF HSs and TP-COF was further analyzed using GITT (Figs. 3e and f, Fig. S12 in Supporting information). As shown in Fig. 3f, the K^+ diffusion coefficient of TP-COF HSs is $10^{-10.7}$ cm^2/s to 10^{-9} cm^2/s, which is higher than the that of TP-COF ($10^{-10.9}$–$10^{-9.4}$ cm^2/s). EIS also shows that the charge transfer resistance (R_{ct}) of TP-COF HSs is smaller than that of TP-COF and the K^+ diffusion coefficient of TP-COF HSs is higher by equivalent circuit fitting (Fig. 3g and Table S2 in Supporting information), which corroborates the results of GITT. After 300 cycles, the R_{ct} of the TP-COF HS electrode increases slightly due to SEI generation, but the diffusion impedance (Z_w) diminishes owing to electrolyte infiltration. Therefore, combined with the special hollow structure, TP-COF HSs display better electrochemical performance because more active sites are exposed and the ion diffusion rate is faster [36].

The TP-COF HS electrodes in selected charge-discharge states were explored by XPS to reveal the K^+ storage mechanism of PIBs (Figs. 3h and i, Fig. S13 in Supporting information). Comparing the C 1s spectra in different states, two peaks at 295.6 and 293.1 eV appear after potassiation, but weaken with depotassiation, signifying the reaction of K^+ and π electrons [37]. In addition, the C–N peak intensity increases and C=N decreases after potassiation and recovers after depotassiation, suggesting a reversible interaction between K^+ and C=N transforming the C–N···K group (Fig. 3i). FTIR and density functional theory calculations (DFT) were performed to further elucidate K^+ storage mechanism.

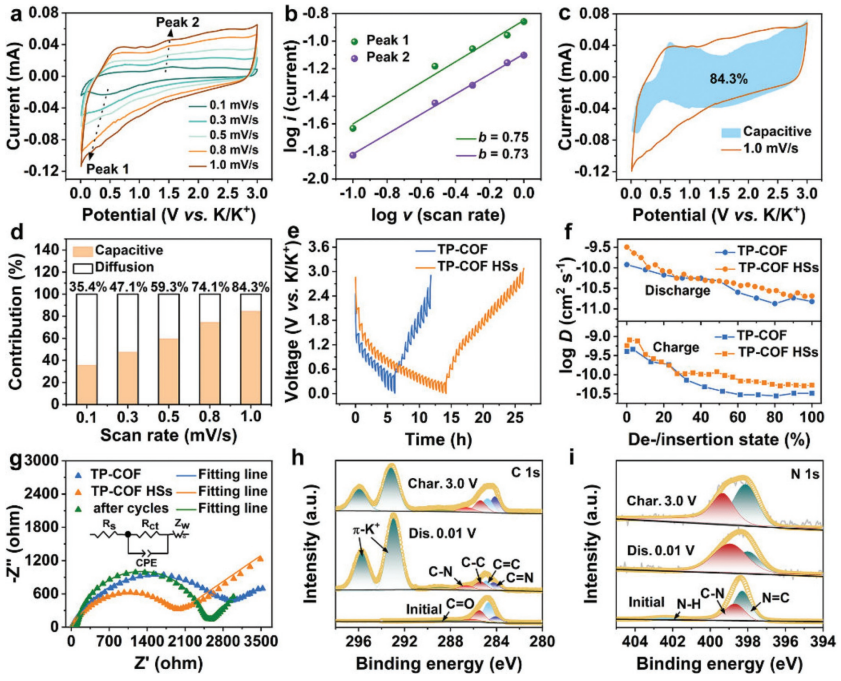

Fig. 3. (a) CV curves of TP-COF HSs from 0.1 mV/s to 1.0 mV/s. (b) Fitting lines of log(peak current) *versus* log(scan rate). (c) Capacitive contribution at 1.0 mV/s and (d) proportions of capacitive contribution at diverse sweep rates. (e) GITT curves of TP-COF and TP-COF HSs and (f) the concerned K^+ diffusion coefficient. (g) Nyquist plots of TP-COF and TP-COF HSs. (h) XPS results of C 1s and (i) N 1s of the TP-COF HS anodes during potassiation/depotassiation.

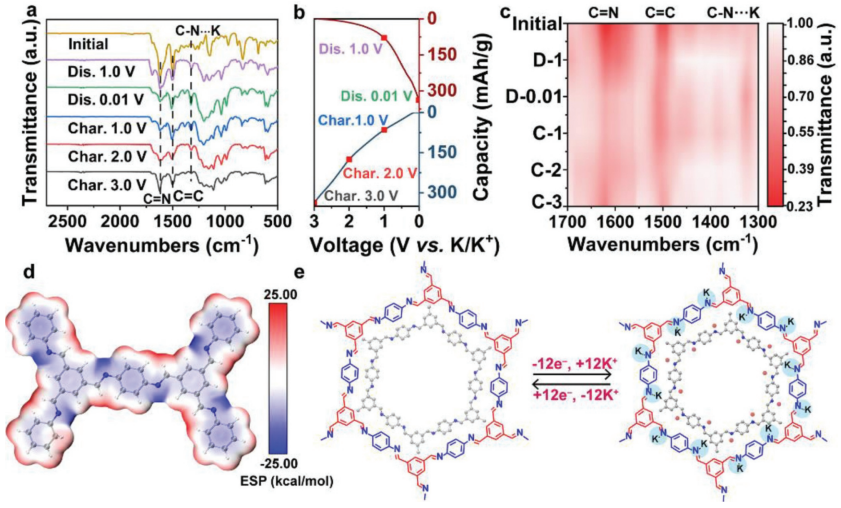

Fig. 4. (a) *Ex-situ* FTIR spectra and (b) charge and discharge profile of TP-COF HSs during potassiation and depotassiation. (c) Locally amplified *ex-situ* FTIR. (d) Electronegativity simulation and (e) structure evolution of TP-COF HSs during charging/discharging.

During the discharge process, the intensity of the C=N group (1618 cm^{-1}) gradually becomes weaker than that of the C=C group (1500 cm^{-1}), and the stretching peak of the C=C group appears red-shifted (Figs. 4a-c). During the subsequent charging process, the strength of the C=N group reverses and progressively increases, confirming that the C=N group is a potassium storage active group. Interestingly, the C–N group (1325 cm^{-1}) intensity increases during K^+ insertion and decreases during K^+ removal, which agrees well with the XPS analysis (Figs. 3h and i). Meanwhile, the new peaks below 1300 cm^{-1} can be assigned to the decomposition deposition of KFSI on the surface of the TP-COF HS electrode (Fig. S14 in Supporting information). DFT calculations based on repeating structural units unveil that C=N is a highly active site for K^+ adsorption by analyzing the electrostatic potential (Fig. 4d). This result justifies the above analysis of the most likely active sites for potassium storage, as depicted in Fig. 4e.

In summary, we have designed hollow spherical imine-based TP-COF as an anode material for PIBs *via* a simple template strategy. The as-synthesized TP-COF HSs manifest excellent potassium storage performance due to its more exposed active sites and good wettability of the electrolyte endowed by the hollow architecture. The combination of *ex-situ* analysis and DFT calculation verifies that the C=N group and benzene are the active sites for K storage. This work puts forward the possibility of further uniform morphology design of COF materials and promotes the further application of COFs in potassium ion storage.

Declaration of competing interest

The authors declare that they have no known competing financial interests or personal relationships that could have appeared to influence the work reported in this paper.

Acknowledgments

This work was supported by the National Natural Science Foundation of China (No. 22179063).

Supplementary materials

Supplementary material associated with this article can be found, in the online version, at doi:10.1016/j.cclet.2023.108233.

References

[1] A.Y.S. Eng, C.B. Soni, Y. Lum, et al., Sci. Adv. 8 (2022) eabm2422.
[2] Q. Pan, Z. Tong, Y. Su, S. Qin, Y. Tang, Adv. Funct. Mater. 31 (2021) 2103912.
[3] D. Bresser, S. Passerini, B. Scrosati, Chem. Commun. 49 (2013) 10545–10562.
[4] X.B. Cheng, R. Zhang, C.Z. Zhao, Q. Zhang, Chem. Rev. 117 (2017) 10403–10473.
[5] Y. Tong, Y. Wu, Z. Liu, et al., Chin. Chem. Lett. 34 (2023) 107443.
[6] X. Kuai, K. Li, J. Chen, et al., ACS Nano 16 (2022) 1502–1510.
[7] Q. Pan, Y. Zheng, Z. Tong, L. Shi, Y. Tang, Angew. Chem. Int. Ed. 60 (2021) 11835–11840.
[8] Y. Wang, D. Ouyang, L. Yang, et al., Chin. Chem. Lett. (2022), doi:10.1016/j.cclet.2022.108095.
[9] B. Ji, F. Zhang, X. Song, Y. Tang, Adv. Mater. 29 (2017) 1700519.
[10] J.C. Pramudita, D. Sehrawat, D. Goonetilleke, N. Sharma, Adv. Energy Mater. 7 (2017) 1602911.
[11] M. Zhou, P. Bai, X. Ji, et al., Adv. Mater. 33 (2021) 2003741.
[12] H. Ding, J. Zhou, A.M. Rao, B. Lu, Natl. Sci. Rev. 8 (2021) nwaa276.
[13] B. Ji, W. Yao, Y. Zheng, et al., Nat. Commun. 11 (2020) 1225.
[14] M.A. Zenaidee, J.A. Loo, Nat. Chem. 14 (2022) 482–483.
[15] Q. Zhang, S. Dong, P. Shao, et al., Science 378 (2022) 181–186.
[16] P. Shang, X. Yan, Y. Li, et al., Chin. Chem. Lett. 34 (2023) 107584.
[17] J. Li, X. Jing, Q. Li, et al., Chem. Soc. Rev. 49 (2020) 3565–3604.
[18] Z. Xiong, B. Sun, H. Zou, et al., J. Am. Chem. Soc. 144 (2022) 6583–6593.
[19] Y.Y. Liu, X.C. Li, S. Wang, et al., Nat. Commun. 11 (2020) 5561.
[20] B. Sun, D. Wang, L. Wan, Sci. China Chem. 60 (2017) 1098–1102.
[21] H. Zhao, G.H. Liu, Y.T. Liu, et al., Nano Res. 16 (2023) 281–289.
[22] Q. Pan, Z. Tong, Y. Su, et al., Adv. Mater. 34 (2022) 2203485.
[23] P. Pachfule, S. Kandmabeth, A. Mallick, R. Banerjee, Chem. Commun. 51 (2015) 11717–11720.
[24] L.R. Ahmed, L. Gilmanova, C.T. Pan, S. Kaskel, A.F.M. El-Mahdy, ACS Appl. Polymer Mater. 4 (2022) 9132–9143.
[25] M.X. Wu, Y.W. Yang, Chin. Chem. Lett. 28 (2017) 1135–1143.
[26] X.X. Tang, L.P. Lv, S.Q. Chen, W.W. Sun, Y. Wang, J. Colloid Interface Sci. 622 (2022) 591–601.
[27] Z. Li, B.Y. Guan, J. Zhang, X.W. Lou, Joule 1 (2017) 576–587.
[28] D. Wu, D. Han, Y. Zhou, et al., Chem. Commun. 58 (2022) 9148–9151.
[29] S.Y. Ding, J. Gao, Q. Wang, et al., J. Am. Chem. Soc. 133 (2011) 19816–19822.
[30] Z. Lei, Q. Yang, Y. Xu, et al., Nat. Commun. 9 (2018) 576.
[31] Z. Long, C. Shi, C. Wu, et al., Nanoscale 14 (2022) 1906–1920.
[32] X. Yang, L. Gong, K. Wang, et al., Adv. Mater. 34 (2022) e2207245.
[33] X.X. Luo, W.H. Li, H.J. Liang, et al., Angew. Chem. Int. Ed. 61 (2022) e202117661.
[34] E.R. Wolfson, L. Schkeryantz, E.M. Moscarello, et al., ACS Appl. Mater. Interfaces 13 (2021) 41628–41636.
[35] X. Li, H. Wang, H. Chen, et al., Chem 6 (2020) 933–944.
[36] W.K. Wang, W.W. Zhao, T.T. Chen, et al., Adv. Funct. Mater. 31 (2021) 2101194.
[37] X. Chen, H. Zhang, C. Ci, W. Sun, Y. Wang, ACS Nano 13 (2019) 3600–3607.